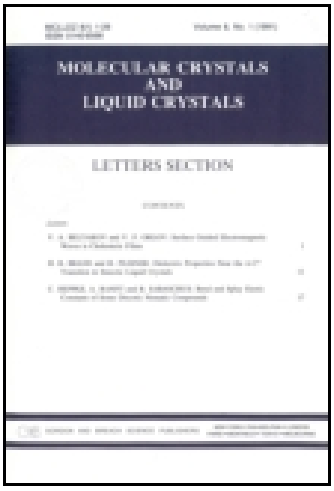

Molecular Crystals and Liquid Crystals
Publication details, including instructions for authors and subscription information:
http://www.tandfonline.com/loi/gmcl20

Construction of Three Novel Coordination Complexes by 3-Nitrophthalic Acid Plus N-Donor Ligands: Synthesis, Structure, and Properties

Ling-yu Zhang[a], Wen-jia Xu[a], Shu-long Wang[a], Gang-hong Pan[a], Zhi-xing Su[b] & Yu Feng[a]

[a] College of Chemistry and Chemical Engineering, Guangxi University for Nationalities, Nanning, P.R. China

[b] , Nanning Bioclone Biotechnology Co., Ltd., Nanning, P.R. China

Published online: 27 May 2014.

To cite this article: Ling-yu Zhang, Wen-jia Xu, Shu-long Wang, Gang-hong Pan, Zhi-xing Su & Yu Feng (2014) Construction of Three Novel Coordination Complexes by 3-Nitrophthalic Acid Plus N-Donor Ligands: Synthesis, Structure, and Properties, Molecular Crystals and Liquid Crystals, 593:1, 214-231, DOI: 10.1080/15421406.2013.874810

To link to this article: http://dx.doi.org/10.1080/15421406.2013.874810

Mol. Cryst. Liq. Cryst., Vol. 593: pp. 214–231, 2014

ISSN: 1542-1406 print/1563-5287 online
DOI: 10.1080/15421406.2013.874810

Construction of Three Novel Coordination Complexes by 3-Nitrophthalic Acid Plus N-Donor Ligands: Synthesis, Structure, and Properties

LING-YU ZHANG,[1] WEN-JIA XU,[1] SHU-LONG WANG,[1] GANG-HONG PAN,[1] ZHI-XING SU,[2] AND YU FENG[1,*]

[1]College of Chemistry and Chemical Engineering, Guangxi University for Nationalities, Nanning, P.R. China
[2]Nanning Bioclone Biotechnology Co., Ltd., Nanning, P.R. China

*In order to explore new coordination frameworks with novel designed 3-nitrophthalic acid and N–donor ancillary ligands, three novel coordination complexes, namely, $[Co_2(3\text{-}NPA)_2(2,2'\text{-}bipy)_2(H_2O)_2]\bullet 2H_2O$ (**1**), $[Mn_2(3\text{-}NPA)_2(4,4'\text{-}bipy)_3(H_2O)_6]\bullet(4,4'\text{-}bipy)$ (**2**), and $[Pb_2O(3\text{-}NPA)]_n$ (**3**) (where $3\text{-}NPAH_2$ = 3-nitrophthalic acid, 2,2′-bipy = 2,2′-bipyridine, 4,4′-bipy = 4,4′-bipyridine), have been hydrothermally synthesized. X-ray structure analysis reveals that **1** and **2** are dinuclear structures, while **3** is a two-dimensional (2D) network polymer. And the hydrogen bonds and π–π stacking also play important roles in affecting the final structure where complexes **1**-**2** have 3D and 2D supramolecular architectures, respectively. These complexes have been characterized by powder X-ray diffractions (PXRD) and thermal gravimetric analyses (TGA). In addition, their photochemical properties have also been investigated.*

Keywords Coordination modes; hydrogen-bonding interactions; N-donor ligands; 3-Nitrophthalic acid

Introduction

The design and synthesis of zero-, one-, two-, or three-dimensional (0D, 1D, 2D, or 3D) coordination assemblies by utilizing directional metal−ligand dative bonds has attracted considerable interest in recent years, which may bring both intriguing architectures and tailor-made applications in such fields as porosity, magnetics, optoelectronics, catalysis, and so on [1, 2]. As it is known, it is still a big challenge to predict the final structures of desired crystalline products, since the self-assembly process of crystalline products is influenced by many factors, such as metal ions, organic ligands, counter ions, solvent system, temperature, and pH of reaction system [3–5]. The delicate balance between the adaptability of the organic ligands with the plentiful and versatile coordination modes of the central metals as well as the coparticipation of counteranions and solvent molecules leads to the formation of either discrete polynuclear complexes or infinite coordination polymers, affording great opportunities for the construction of novel and unusual metal−organic crystalline materials [6, 7]. In order to obtain new coordination complexes with various

*Address correspondence to Yu Feng, College of Chemistry and Chemical Engineering, Guangxi University for Nationalities, Nanning 530006, P.R. China. Tel./Fax: 0771-5360285. E-mail: fengyu771@126.com

topological structures, multicarboxylates are often selected as bridging ligands to construct coordination complexes not only due to their versatile coordination modes to metal centers but also their strong ability to act as hydrogen bonding acceptors and donors [8–11]. Especially, the 3-nitrophthalic acid can serve as excellent candidates for building highly connected or helical coordination frameworks due to their versatile bridging fashions [12, 13]. Apart from the carboxylate linkers, N-donor ligands are frequently used as ancillary ligands to give multipodal anions acting as bridging, chelating, and charge balance ligands for synthesizing polynuclear species [14]. Moreover, the hybrid coordination complexes constructed by 3-nitrophthalic acid are rarely documented to date. With this understanding, 3-$NPAH_2$ (3-nitrophthalic acid) was chosen as the organic ligands, 2,2′-bipy and 4,4′-bipy were chosen as neutral co-ligands to construct new coordination complexes under the hydrothermal reaction. This paper presents the syntheses, structures, thermal stabilities, luminescent properties, and powder X-ray diffraction (PXRD) of three new coordination complexes $[Co_2(3\text{-}NPA)_2(2,2'\text{-}bipy)_2(H_2O)_2]\bullet 2H_2O$ (**1**), $[Mn_2(3\text{-}NPA)_2(4,4'\text{-}bipy)_3(H_2O)_6]\bullet(4,4'\text{-}bipy)$ (**2**), and $[Pb_2O(3\text{-}NPA)]_n$ (**3**).

Experimental

All chemicals were commercial materials of analytical grade and used without purification. Elemental analysis for C, H, and N was carried out on a Perkin–Elmer 2400 II elemental analyzer. The FT-IR spectrum was obtained on a PE Spectrum One FT-IR Spectrometer Fourier transform infrared spectroscopy in the 4000–400 cm^{-1} regions, using KBr pellets. Perkin–Elmer Diamond TG/DTA thermal analyzer was used to record simultaneous TG and DTG curves in the static air atmosphere at a heating rate of 10 K min^{-1} in the temperature range 25 to 1000 °C using platinum crucibles. Fluorescence spectra were recorded with F-2500 FL Spectrophotometer analyzer. PXRD patterns were obtained using a pinhole camera (Anton Paar) operating with a point-focused Ni-filtered Cu Kα radiation in the 2θ range from 5° to 50° with a scan rate of 0.08° per second.

Synthesis of Complex $[Co_2(3\text{-}NPA)_2(2,2'\text{-}bipy)_2(H_2O)_2]\bullet 2H_2O$ (1)

The reagents of $CoCl_2$ (0.129 g, 1.00 mmol), 3-$NPAH_2$ (0.106 g, 0.500 mmol), and 2,2′-bipy (0.0781 g, 0.500 mmol) were dissolved in 15 mL-mixed solvent of DMF/H_2O (volume ratio 1:2) and then stirred for 0.5 hr. Then an aqueous solution of sodium hydroxide was added dropwise with stirring to adjust the pH value of the solution being 6. The resulting mixture was sealed in a 30 mL Teflon-lined stainless reactor, kept under autogenous pressure at 145 °C for 72 hr, and then slowly cooled to room temperature at a rate of 5 °C per hr. The block crystals suitable for X-ray diffraction were isolated directly (Yield: 60%, based on Co). Anal. Calcd. for $C_{36}H_{30}Co_2N_6O_{16}$ (%): C, 46.97; H, 3.28; N, 9.13. Found: C, 46.84; H, 3.20; N, 9.28. IR data (KBr pellets, cm^{-1}): 3447(s), 3081(m), 1601(vs), 1576(s), 1542(w), 1522(vs), 1476(w), 1458(m), 1442(w), 1403(s), 1383(s), 1338(s), 1074(w), 1023(w), 924(m), 830(w), 767(m), 735(w), 718(m), 668(s), 652(w).

Synthesis of Complex $[Mn_2(3\text{-}NPA)_2(4,4'\text{-}bipy)_3(H_2O)_6]\bullet(4,4'\text{-}bipy)$ (2)

A solution of 3-$NPAH_2$ (0.106 g, 0.500 mmol) in 3 mL DMF was added dropwise with stirring at room temperature to a solution of $MnCl_2{\cdot}4H_2O$ (0.198 g, 1.00 mmol) in the

mixture of 10 mL water and 5 mL ethanol. Then an aqueous solution of sodium hydroxide was added dropwise with stirring to adjust the pH value of the solution being 6. The resulting mixture was sealed in a 30 mL Teflon-lined stainless reactor, kept under autogenous pressure at 150 °C for 72 hr, and then slowly cooled to room temperature at a rate of 5 °C per hr. The block crystals of **2** were obtained in 65% yield based on Mn. Anal. Calcd. for $C_{56}H_{50}Mn_2N_{10}O_{18}$ (%): C, 53.34; H, 4.00; N, 11.11. Found: C, 53.21; H, 3.92; N, 11.26. IR data (KBr pellets, cm^{-1}): 3056(s), 1602(vs), 1555(w), 1530(s), 1489(w), 1450(w), 1381(s), 1343(m), 1218(w), 1067(w), 1003(w), 812(s), 750(w), 624(m).

Synthesis of Complex $[Pb_2O(3\text{-}NPA)]_n$ (3)

The same synthetic procedure as that for **1** was used except that 2,2′-bipy was not added, $CoCl_2$ (0.129 g, 1.00 mmol) was replaced by $Pb(NO_3)_2$ (0.331 g, 1.00 mmol). The block crystals suitable for X-ray diffraction were isolated directly, washed with ethanol and dried in air (Yield: 60%, based on Pb). Anal. Calcd. for $C_8H_3Pb_2NO_7$ (%): C, 15.02; H, 0.47; N, 2.19. Found: C, 15.01; H, 0.48; N, 2.17. IR data (KBr pellets, cm^{-1}): 1611(w), 1574(m), 1529(s), 1461(m), 1391(m), 1370(w), 1344(s), 847(w), 787(w), 755(w), 712(m), 689(w).

Crystal Structure Determination

Suitable single crystal with approximate dimensions were mounted on a glass fiber and used for X-ray diffraction analyses. Data were collected at 293 (2) K on a Bruker Apex CCD diffractometer using the ω scan technique with Mo $K\alpha$ radiation ($\lambda = 0.71069$ Å). Absorption corrections were applied using the multi-scan technique [15]. The structures were solved by the Direct Method and refined by full-matrix least-square techniques on F^2 using SHELXL-97 [16]. All nonhydrogen atoms were refined anisotropically. The crystal data and structure refinement details for three complexes are shown in Table 1. Selected bond lengths and angles of the complexes are listed in Table 2, and possible hydrogen bond geometries are given in Table 3.

Results and Discussion

Description of the Structure Description of the Structure

The single-crystal X-ray diffraction analysis reveals that complexes **1** and **2** crystallize in the triclinic *P-1* space group, and **3** belongs to the orthorhombic system with space group *Cmca*.

The asymmetric unit of **1** consists of one Co(II) ion , one 3-NPA^{2-}, one 2,2′-bipy, one coordinated water molecule and one lattice water molecule. As depicted in Fig. 1, there are two deprotonated 3-nitrophthalic acid coordinated by two neighboring Co(II) cations on the symmetrical position, forming a 14-membered ring, and two carboxylate groups of 3-NPA^{2-} ligand adopt different coordination modes: one carboxylate group adopts $\mu 1$–η^1:η^0 mode and the other adopts $\mu 1$–η^1:η^1 mode (Supplementary Fig. S1a). The Co1 cation adopts a distorted octahedral geometry by coordinating to three carboxylate oxygen atoms from two neighboring 3-NPA^{2-} ligands, two nitrogen atoms from one 2,2-bipy, and one oxygen atom from one coordinated water. The atoms (O6, N1) occupy the axial positions, and the nitrogen atom (N2) and oxygen atoms (O7, O8, and O4#1) comprise the equatorial plane. The Co–O bond distances vary from 2.037 (2) to 2.373 (3) Å, while the Co–N bond lengths are 2.114 (3) and 2.141 (3) Å, and all in the reasonable range [17]. The structure is

Table 1. Experimental data for complexes **1**, **2**, and **3**

Complexes	**1**	**2**	**3**
Empirical formula	$C_{36}H_{30}Co_2N_6O_{16}$	$C_{56}H_{50}Mn_2N_{10}O_{18}$	$C_8H_3NO_7Pb_2$
Formula weight	920.52	1260.94	639.49
Temperature	296 (2) K	296 (2) K	296 (2) K
Wavelength	0.71073 Å	0.71073 Å	0.71073 Å
Crystal system, space group	Triclinic, *P*-1	Triclinic, *P*-1	Orthorhombic, *Cmca*
a (Å)	7.4988 (13)	10.725 (4)	5.737 (2)
b (Å)	10.4760 (18)	11.313 (4)	13.882 (5)
c (Å)	12.192 (2)	12.758 (4)	27.878 (10)
α (°)	88.281 (2)	78.335 (4)	90.000 (2)
β (°)	75.012 (2)	70.199 (4)	90.0000 (10)
γ (°)	77.361 (2)	86.222 (5)	90.0000 (10)
Volume (Å^3)	902.4 (3)	1426.4 (8)	2220.2 (14)
Z	1	1	8
$D_{calc.}$ (Mg·m^{-3})	1.694	1.468	3.826
Absorption coefficient (mm^{-1})	1.007	0.526	30.318
F (000)	470	650	2224
Crystal size	0.26 × 0.23 × 0.22	0.25 × 0.24 × 0.23	0.22 × 0.21 × 0.20
θ range for data collection (°)	1.73 to 25.00	1.73 to 25.00	1.46 to 25.00
Reflections collected	4944	7581	5629
Unique reflections	3127 [R(int) = 0.0203]	4941 [R(int) = 0.0263]	1080 [R(int) = 0.0780]
Completeness to $\theta = 25.00$	98.3%	98.3%	99.8%
Absorption correction	Semi-empirical from equivalents	Semi-empirical from equivalents	Semi-empirical from equivalents
Max. and min. transmission	0.8088 and 0.7797	0.8887 and 0.8798	0.0645 and 0.0574
Data/restraints/parameters	3127/0/271	4941/18/388	1080/162/105
Goodness-of-fit on F^2	1.055	1.024	1.209
R indices [$I > 2\sigma(I)$]	$R1 = 0.0411$, $wR2 = 0.1216$	$R1 = 0.0528$, $wR2 = 0.1497$	$R1 = 0.0630$, $wR2 = 0.1701$
R indices (all data)	$R1 = 0.0494$, $wR2 = 0.1378$	$R1 = 0.0668$, $wR2 = 0.1643$	$R1 = 0.0646$, $wR2 = 0.1716$
Largest diff. peak and hole (e.Å^{-3})	0.703 and −0.532	0.650 and −0.419	1.681 and −6.246

Table 2. Selected bond lengths (Å) and angles (°) for **1**, **2**, and **3**

	Complex **1**		
Co(1)–O(4)#1	2.037(2)	Co(1)–N(2)	2.141(3)
Co(1)–O(6)	2.095(2)	Co(1)–N(1)	2.114(3)
Co(1)–O(7)	2.088(2)	Co(1)–O(8)	2.373(3)
O(4)#1–Co(1)–O(7)	96.73(9)	O(7)–Co(1)–O(6)	94.20(10)
O(4)#1–Co(1)–O(6)	87.53(9)	O(7)–Co(1)–N(1)	99.84(10)
O(7)–Co(1)–O(8)	58.48(9)	O(4)#1–Co(1)–N(2)	91.29(10)
O(6)–Co(1)–O(8)	83.28(9)	N(2)–Co(1)–O(8)	113.81(10)
N(1)–Co(1)–O(8)	85.26(9)	N(1)–Co(1)–N(2)	76.30(11)
O(4)#1–Co(1)–O(8)	152.59(9)	O(6)–Co(1)–N(2)	86.81(11)
O(4)#1–Co(1)–N(1)	112.53(9)	O(6)–Co(1)–N(1)	153.68(11)
O(7)–Co(1)–N(2)	171.94(9)		
	Complex **2**		
Mn(1)–O(4)	2.144(2)	Mn(1)–O(7)	2.162(2)
Mn(1)–O(8)	2.183(2)	Mn(1)–N(2)	2.271(3)
Mn(1)–O(9)	2.195(2)	Mn(1)–N(4)	2.281(3)
O(4)–Mn(1)–O(9)	87.43(9)	O(7)–Mn(1)–O(9)	91.73(10)
O(7)–Mn(1)–O(8)	83.15(9)	O(7)–Mn(1)–N(4)	93.19(10)
O(4)–Mn(1)–N(4)	89.72(9)	O(8)–Mn(1)–O(9)	99.58(10)
O(4)–Mn(1)–O(8)	83.16(9)	O(7)–Mn(1)–N(2)	92.51(10)
O(4)–Mn(1)–O(7)	165.95(9)	O(9)–Mn(1)–N(2)	85.72(10)
O(8)–Mn(1)–N(2)	173.21(9)	O(4)–Mn(1)–N(2)	101.41(10)
O(8)–Mn(1)–N(4)	88.93(10)	O(9)–Mn(1)–N(4)	170.64(10)
N(2)–Mn(1)–N(4)	86.10(10)		
	Complex **3**		
Pb(1)–O(5)	2.301(4)	Pb(2)–O(6)	2.717(5)
Pb(2)–O(5)	2.304(4)	Pb(1)–O(6)	2.559(5)
Pb(2)–O(4)#4	2.460(7)	O(4)#4–Pb(2)–O(6)	138.31(11)
O(6)#2–Pb(1)–O(6)	51.3(2)	O(5)–Pb(1)–O(6)	74.79(12)
O(5)–Pb(1)–O(5)#1	76.6(2)	O(5)–Pb(2)–O(6)	71.67(12)
O(5)–Pb(2)–O(5)#3	77.5(2)	O(6)–Pb(2)–O(6)#5	80.8(2)
Pb(2)–O(5)–Pb(2)#3	102.5(2)	Pb(1)–O(5)–Pb(1)#1	103.4(2)
Pb(1)–O(5)–Pb(2)	116.66(2)	O(5)–Pb(1)–O(6)#2	105.94(12)
Pb(1)–O(5)–Pb(2)#3	109.10(3)	O(5)–Pb(2)–O(6)#5	119.76(12)
O(5)#1–Pb(1)–O(6)#2	74.79(11)	O(5)–Pb(2)–O(4)#4	74.40(13)
Pb(1)–O(6)–Pb(2)	95.91(15)		

Note: Symmetry transformations used to generate equivalent atoms for **1**: #1 −x+1, −y, −z+1; for **3**: #1 −x, −y+1, −z+2; #2 −x, y, z #3 −x+1, −y+1, −z+2 #4 −x+1/2, −y+3/2, −z+2 #5 −x+1, y, z.

stabilized by intermolecular O–H···O and C–H···O hydrogen bonds (Table 3). The crystal structure is further connected through face-to-face π–π stacking between two adjacent 3-NPA^{2-}. Two adjacent 2,2′-bipy and two adjacent 3-NPA^{2-} molecules are completely parallel with a interplanar separation of ca. 3.5995 (4) and 3.6409 (5) Å, respectively. The molecules stack with each other via perfect face-to-face π–π interaction and C–H···O

Table 3. Hydrogen-bond geometry (Å) and angles (°) for complexes

D-H···A	Symmetry code	D–H	H···A	D···A	D–H···A
	Complex **1**				
O1–H(1A)···O(7)	−x + 1, −y + 1, −z + 1	0.85	2.06	2.894(4)	168
O1–H(1B)···O(5)	x, y + 1, z	0.85	2.40	2.861(4)	114
O1–H(1B)···O(8)	−x + 2, −y + 1, −z + 1	0.85	2.57	3.344(4)	153
O(6)–H(6A)···O(5)	−x + 2, −y, −z + 1	0.85	2.34	2.777(3)	113
O(6)–H(6B) ···O(5)		0.85	2.41	2.777(3)	107
C(3)–H(3)···O(3)		0.93	2.53	3.347(5)	147
C(4)–H(4)···O(8)		0.93	2.57	3.436(5)	156
C(7)–H(7)···O(8)		0.93	2.52	3.339(4)	147
C(10)–H(10)···O(6)		0.93	2.50	3.017(4)	115
	Complex **2**				
O(7)–H(7C)···O(1)	−x + 1, −y + 2, −z + 1	0.85	1.86	2.705(4)	176
O(7)–H(7D)···N(3)	−x + 2, −y + 2, −z + 2	0.85	1.93	2.784(5)	177
O(8)–H(8C)···O(2)	−x + 1, −y + 2, −z + 1	0.85	1.86	2.705(3)	173
O(8)–H(8D)···O(2)		0.85	1.88	2.727(3)	173
O(9)–H(9D)···N(5)	−x + 1, −y + 2, −z + 1	0.85	1.96	2.809(5)	178
O(9)–H(9E)···O(3)		0.85	1.82	2.670(3)	177
	Complex **3**				
C(1)–H(1)···O(2)		0.93	2.31	2.646(13)	101
C(3)–H(3)···O(4)		0.93	2.43	2.781(14)	102

hydrogen bonds [C4–H4···O8 = 2.566 (2), C7–H7···O8 = 2.518 (3) Å] in arrays to form a 2D supramolecular structure (Fig. 2). Moreover, the resulting 2D structure is cross-linked by hydrogen-bond interactions between O–H groups from lattice waters and carboxylate oxygen atoms (O1–H1···O7 = 2.057 (2), O17–H1···O8 = 2.565 (3) Å, thus leading to the formation of a 3D supramolecular architecture (Fig. 3).

The asymmetric unit of **2** contains one Mn(II) ion, one 3-NPA^{2-} anion, one and a half 4,4′-bipy, three coordinated water molecules, and a half lattice 4,4′-bipy. There is an obvious difference of the coordination modes of the 3-NPA^{2-} ligand in **1** and **2** (Supplementary Figs. S1a and S1b). The carboxylate group of the 3-NPA^{2-} ligand adopts $\mu 1$–η^1:η^0 coordination mode. As shown in Fig. 4, the coordination environment around the Mn1 ion is best portrayed as a distorted [MnN_2O_4] octahedral geometry, ligated by one oxygen atom (O9) from a coordinated water molecule and one nitrogen atom (N4) from one 4,4′-bipy at the axial sites, one oxygen atom (O4) from one 3-NPA^{2-}, and two oxygen atoms (O7, O8) from two coordinated water molecules as well as one pyridyl nitrogen atom (N3) in the equatorial

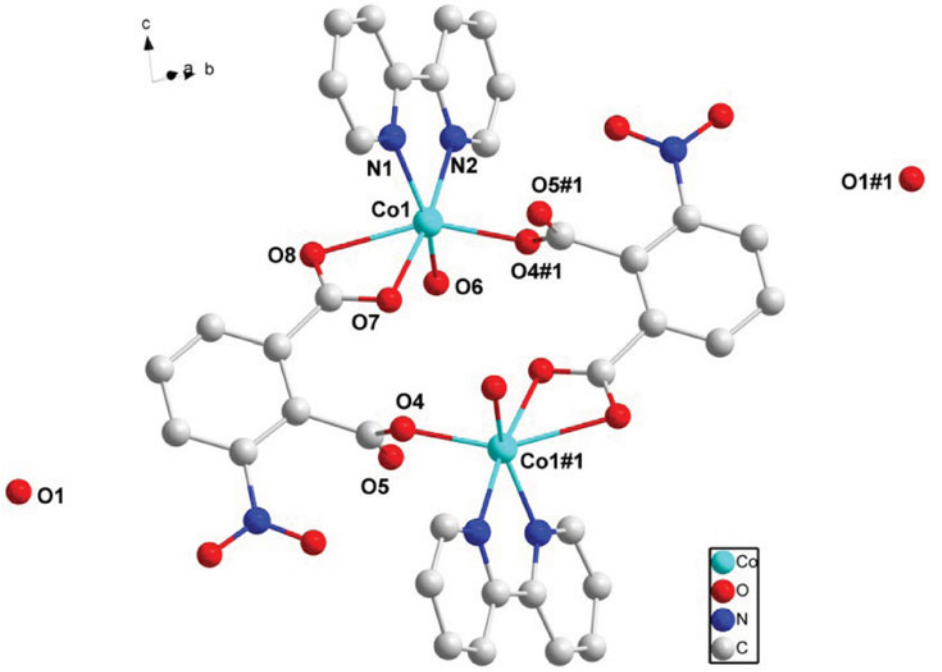

Figure 1. The coordination environment of Co(II) ion of the complex 1. All the hydrogen atoms are omitted for clarity. Symmetry codes: #1 = −1 + x, y, −1 + z.

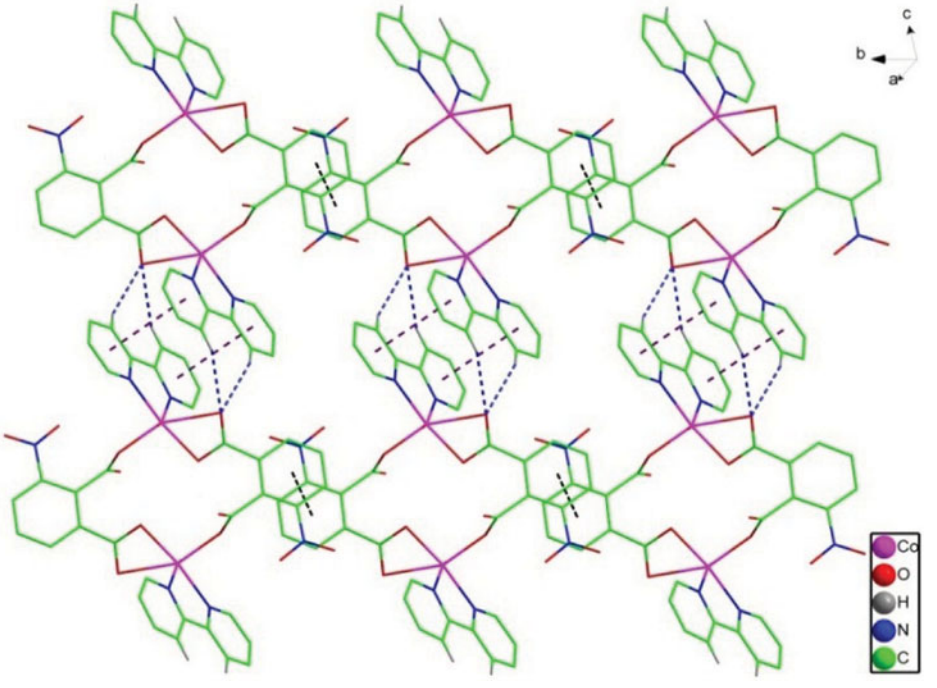

Figure 2. The 2D-layered network of complex 1 via H-bonding and π–π stacking interactions. Unnecessary atoms are omitted for clarity.

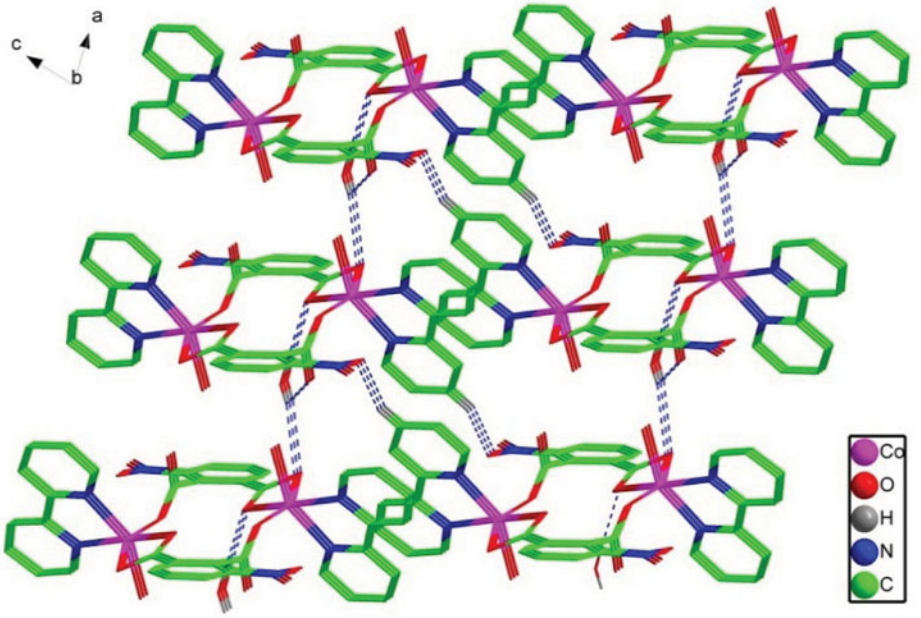

Figure 3. The 3D supramolecular structure of complex 1 via H-bonding. Unnecessary atoms are omitted for clarity.

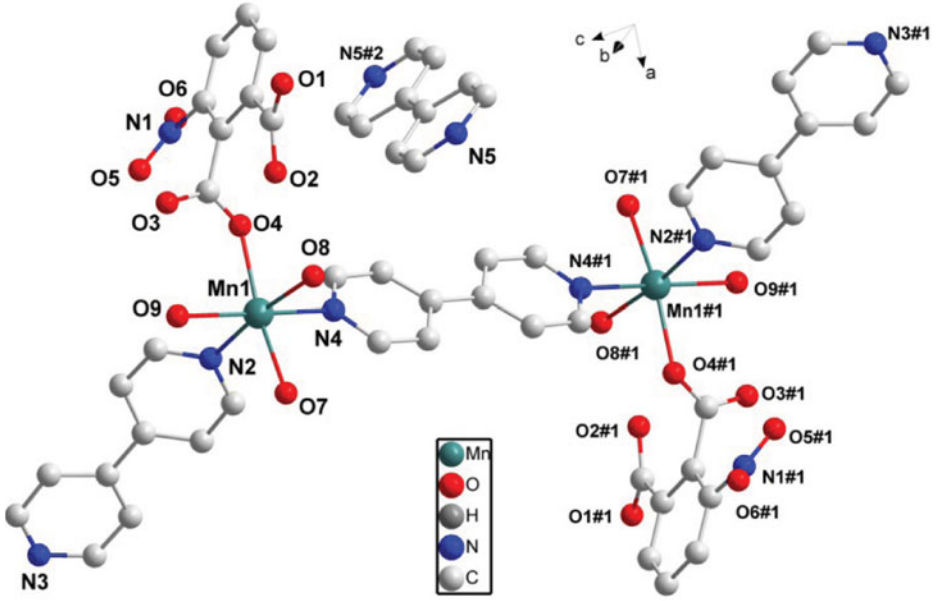

Figure 4. The coordination environment of Mn(II) ion of the complex 2. All the hydrogen atoms are omitted for clarity. Symmetry codes: #1 = 2−x, 1−y, 1−z; #2 = 1−x, 1−y, 1−z.

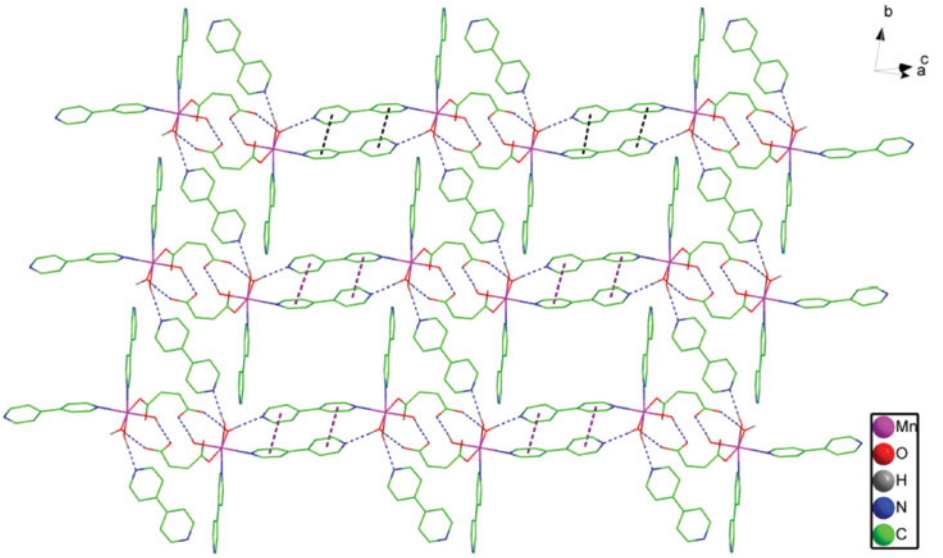

Figure 5. The 2D-layered network of complex 2 via H-bonding and π–π stacking interactions. Unnecessary atoms are omitted for clarity.

plane. The O–H···O and O–H···N hydrogen bondings play an important role in stabilizing the crystal structure (Table 3). Two adjacent 4,4′-bipy molecules are connected by π–π stacking interactions with a distance of 3.733 (2) Å. The binuclear clusters are further extended by π–π stacking interactions and O–H···N hydrogen-bonding [O7–H7C···N3 = 1.935 (5), O9–H9D···N5 = 1.959 (4) Å] as well as O–H···O nonclassical hydrogen bonds [O7–H7C···O1 = 1.857 (3), O8–H8C···O2 = 1.860 (2) Å] into a 2D supramolecular framework (Fig. 5). It is not doubtful for these hydrogen bonding interactions to contribute significantly to the alignment of the molecules in the crystalline state.

As shown in Fig. 6, the asymmetric unit of **3** is composed of two Pb(II) ions, one 3-NPA^{2-} anion and a μ4-O. In complex **3**, there are two different kinds of metal centers in which Pb1 is coordinated to three carboxylate oxygen atoms (O6, O6#1, and O3#6) from two 3-NPA^{2-} and two μ4-oxygen atoms (O5, O5#3), whereas Pb2 ion possesses a five-coordinated sphere but the difference in this is coordinated by three carboxylate oxygen atoms (O6, O6#2, and O4#5) from three different 3-NPA^{2-}. The average Pb1–O and Pb2–O distances are 2.404 (2) and 2.466 (6) Å, respectively, both of which are in the normal range. The four Pb(II) ions form a tetranuclear unit $[Pb_4(\mu4\text{-}O)_2]^{4+}$ through bonding from one bridging μ4-O. This irregular polyhedron Pb_4O_2 cluster is rarely documented in the literature [18]. Each cluster is linked to two neighboring ones by two 3-NPA^{2-} ligands. The coordination modes of 3-NPA^{2-} are shown in Supplementary Fig. S1c, and the 3-NPA^{2-} ligand shows $\mu5$–η^2:η^2:η^1:η^1 coordination mode in bridging fashion. Bonding of the 3-NPA^{2-} ligands to the Pb_4O_2 clusters leads to a 2D network structure (Fig. 7). Notably, the open framework in **3** is sustained exclusively by 1D metal cluster chain running along the *ac*-direction as shown in Fig. 8. This packing gives rise to rhombic-shaped channels with a dimension of ca. 2.3039 (36) × 2.3039 (36) Å^2 and 2.3012 (36) × 2.3012 (36) Å^2. The weaker nonclassical hydrogen bonds were observed between C–H moieties and the coordinated carboxylate oxygen atom (O4) as well as the uncoordinated carboxylate

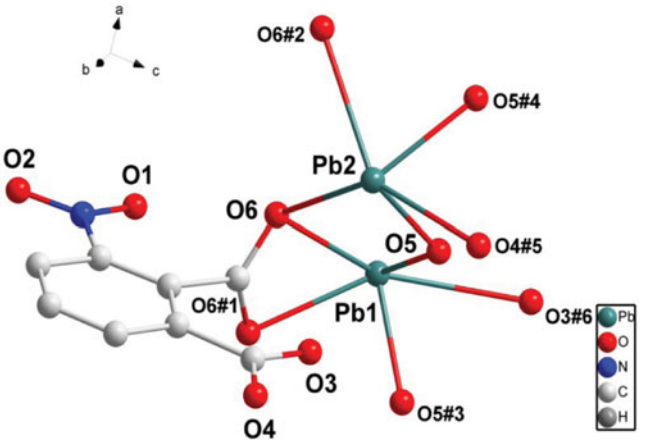

Figure 6. Coordination environment of Pb(II) ion of the complex 3. All the hydrogen atoms are omitted for clarity. Symmetry codes: #1 = −x, y, z; #2 = 1−x, y, z; #3 = −x, 1−y, 2−z; #4 = 1−x, 1−y, 2−z; #5 = 0.5 + x, 1.5−y, 2−z; #6 = x, 1−y, 2−z.

oxygen atom (O2), with the distances of 2.309 (1) and 2.434 (5) Å. The extensive hydrogen bonds may contribute for the stability of the MOF.

Comparison of the Structures

It is known that multicarboxylate ligands have been proved to be excellent structural constructors due to their various coordination modes [19]. The different structures of the complexes **1**–**3** indicate that the multicarboxylate ligand have great influence on the structures of the complexes due to their different coordination modes. Therefore, comparison and comprehension of the coordination modes of the carboxylate ligand are a good and feasible method to predesign the coordination complexes. There are three kinds of coordination modes of 3-NPA^{2-} in the complexes **1**–**3** described above (Supplementary Fig. S1). In complex **1**, each 3-NPA^{2-} anions link two Co(II) cations in a $\mu 2$–η^1:η^1:η^1:η^0 coordination mode (Supplementary Fig. S1a) to gain 0D molecular rings. However, in complex **2**, each 3-NPA^{2-} anion coordinates one Mn(II) cation, displaying a $\mu 1$–η^1:η^0:η^0:η^0 coordination mode (Supplementary Fig. S1ba), yielding a 0D molecular chains. Interestingly, in **3**, each 3-NPA^{2-} anion links five Pb(II) cations in a $\mu 5$–η^2:η^2:η^1:η^1 coordination mode; in the coordination mode, the 3-NPA^{2-} anions bridge the Pb(II) cations to form a 2D network structure. On the basis of the above description, it can be seen that the variations in the coordination modes of 3-NPA^{2-} anions can result in the structure difference of the compounds.

From the structural descriptions above, it can be seen that the N-donor ligands also have a significant effect on the construction of various structures. The introduction of the chelating 2,2′-bipy ligand generally results in drastic change of the structures. In **3**, the 3-NPA^{2-} anions bridge divalent metal cations to gain a 2D layer. However, when 2,2′-bipy is introduced into the reaction system of **3**, a 0D dimeric structure is obtained. The formation of the low dimensional structure of **1** may be attributable to the steric hindrance of the chelating 2,2′-bipy ligand. From the results above, we can see that the N-donor ligands play an important role in the formation of the final complex structures. In addition, the hydrogen

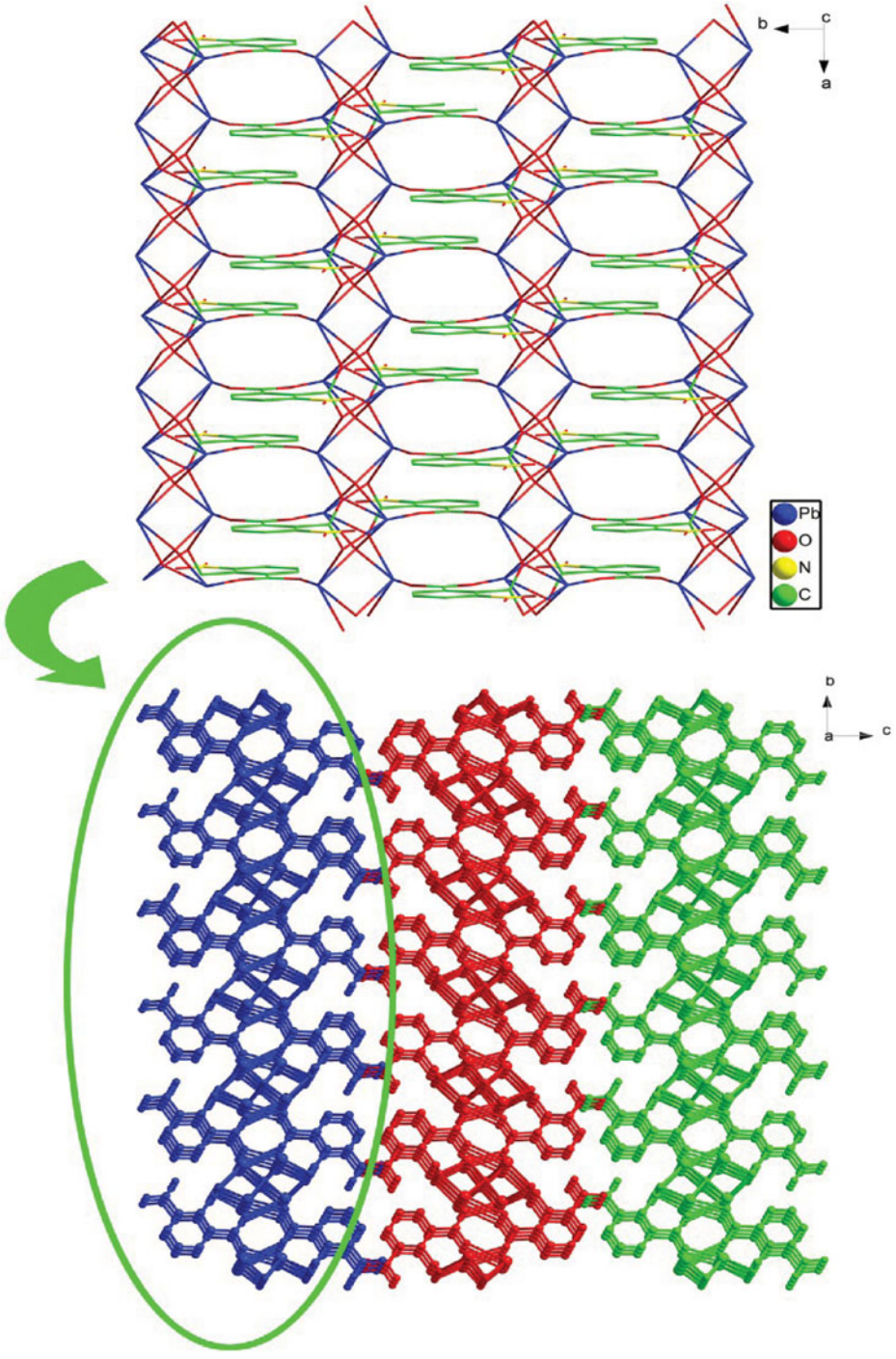

Figure 7. The 2D-layered network of complex 3. Unnecessary atoms are omitted for clarity.

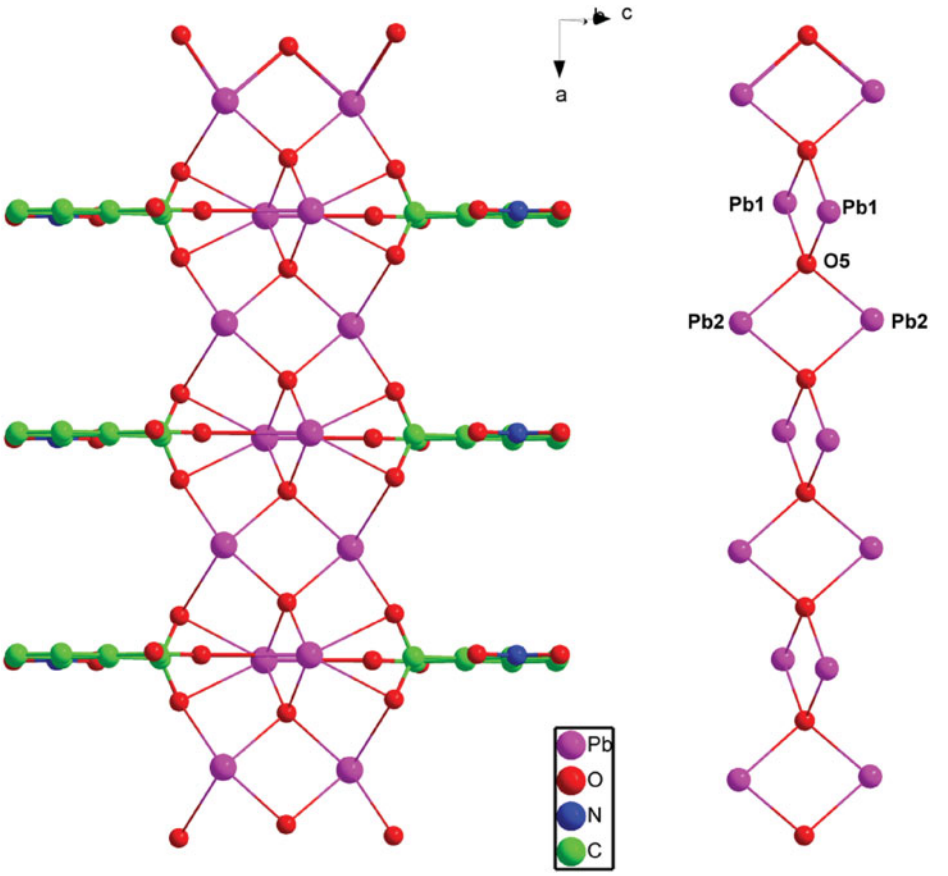

Figure 8. View of one-dimensional infinite metal cluster chain in complex 3.

bonds and π–π stacking also play important roles in affecting the final structures where complexes **1** and **2** have 3D and 2D supramolecular architectures, respectively.

IR Spectrum

In the IR spectra of the complexes **1** and **2**, the strong and broad bands at about 3500–3000 cm^{-1} region are attributed to the symmetric O–H stretching modes and O–H bending modes, respectively. $\upsilon_{as}COO$ appears strong peaks at 1601 and 1576 cm^{-1} in complex **1**, 1602 and 1555 cm^{-1} in **2**, and 1611 and 1574 cm^{-1} in **3**. $\upsilon_{s}COO$ appears peaks at 1403 and 1383 cm^{-1} in **1**, 1450 and 1381 cm^{-1} in **2**, and 1461 and 1391 cm^{-1} in **3**. For complex **1**, the strong peak at 1542 cm^{-1} is attributed for $\upsilon_{as}NO_2$ and additional peaks at 1338 and 1522 cm^{-1} are attributed for $\upsilon_{s}NO_2$ and C=N. For complex **2**, the strong peak at 1530 is attributed for $\upsilon_{as}NO_2$ and additional peaks at 1343 and 1489 cm^{-1} are consistent with $\upsilon_{s}NO_2$ and C=N. In addition, for complex **3**, the strong peak at 1529 is attributed for $\upsilon_{as}NO_2$ and the additional peak at 1344 cm^{-1} is consistent with $\upsilon_{s}NO_2$.

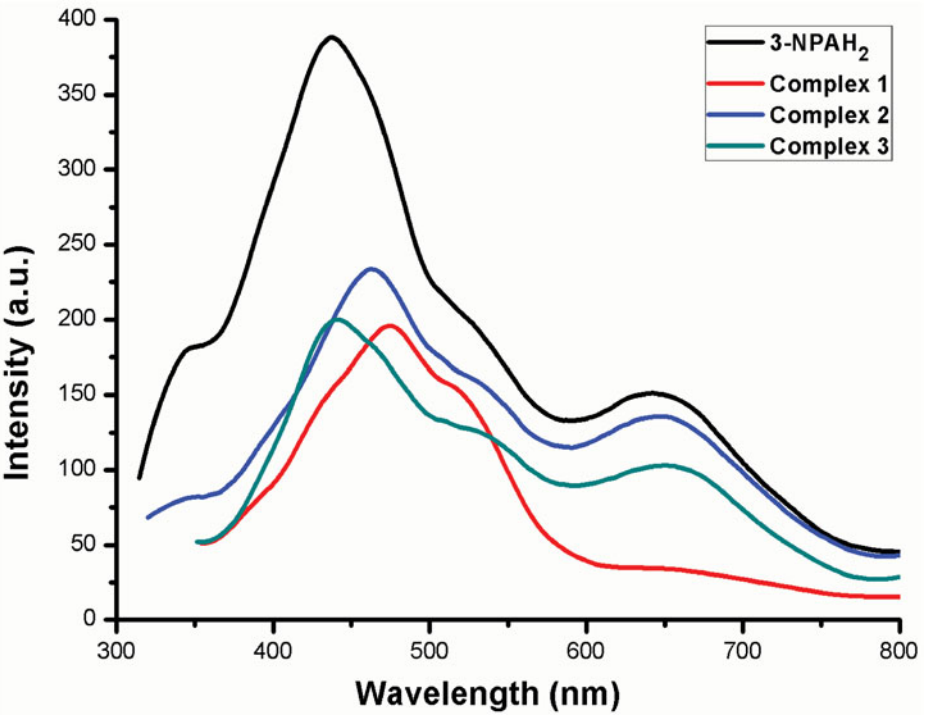

Figure 9. Solid-state fluorescent emission spectra of 3-NPAH2 (black), complex 1 (red), complex 2 (blue), and complex 3 (green) at room temperature.

XRD Patterns

To confirm the phase purity of the bulk materials, PXRD experiments have been carried out for complexes **1**–**3**. The XRPD experimental and computer-simulated patterns of the corresponding complexes are shown in Supplementary Fig. S2. Although the experimental patterns have a few un-indexed diffraction lines and some are slightly broadened in comparison with those simulated from the single-crystal models, it can be still well considered that the bulk synthesized materials and the crystals used for diffraction are homogeneous.

Fluorescence Properties

Luminescent complexes are of great interest due to their various applications in chemical sensors, photochemistry, and light-emitting diodes (LEDs) [20, 21]. Hence, the solid state photoluminescence properties of 3-$NPAH_2$ ligand and complexes **1**–**3** were investigated at room temperature (Fig. 9) under the same experimental conditions. In the solid state, the strongest emission peak for the free ligand 3-$NPAH_2$ is at 438 nm with the excitation peak at 233 nm, which is attributed to the π^*–n transitions [22]. The strongest excitation peaks for **1**–**3** are at 285, 230, and 255 nm, emission spectra mainly show strong peaks at 474, 462, and 441 nm, respectively. The ligand chelation to the metal center may effectively increase the rigidity of the ligand and reduce the loss of energy by radiationless decay, thus causing the red shift in **1, 2,** and **3**. Therefore, the luminescence behavior of complexes is caused by metal ligand charge transfer (MLCT) [23].

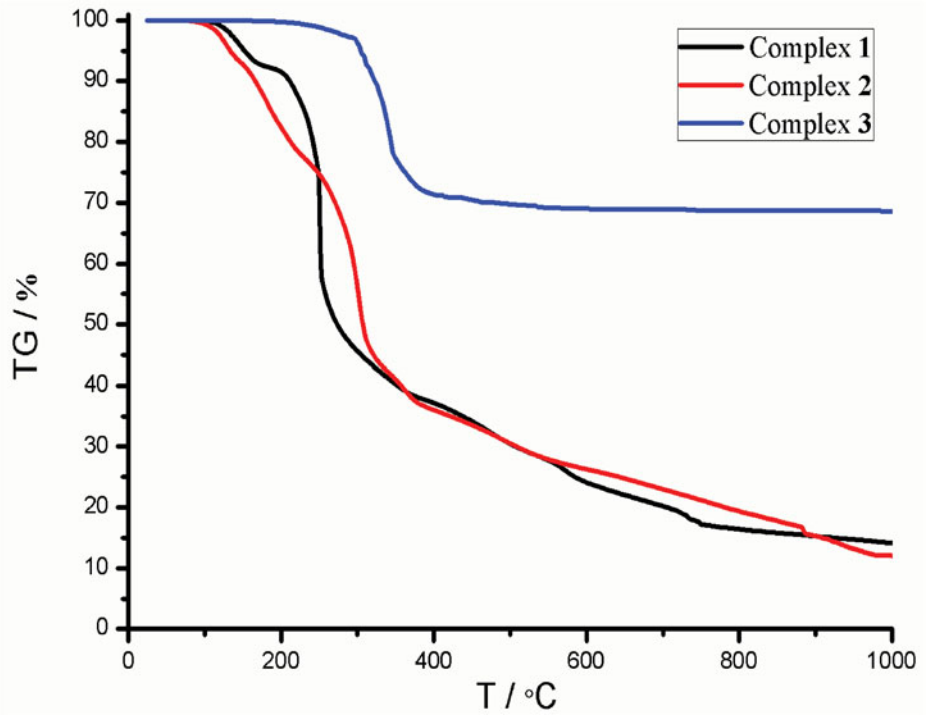

Figure 10. The TG curves of three complexes.

Thermogravimetric (TG) Analyses

In order to study the framework stability of the title complexes, the thermogravimetric (TG) analysis was performed in N_2 atmosphere on polycrystalline samples of complexes **1–3**, and the TG curves are shown in Fig. 10. The TG curve of **1** shows the first loss of 7.79% in the temperature range of 89 to 186 °C, which indicates the exclusion of watermolecules and coordinated water molecules (calcd., 7.83%); The second stage occurs between 187 and 251 °C, the anhydrous complex loses 33.89% of total weight, which is due to the decomposition of two 2,2′-bipy (calcd., 33.93%). The final weight loss of 44.08% (calcd., 45.43%) corresponds to the loss of two 3-NPA^{2-} in the temperature range of 252 to 991 °C. The remaining residue corresponds to the formation of CoO (obsd., 14.24%; calcd., 16.28%).

For **2**, the weight loss attributed to the gradual release of coordinated water molecules is observed in the range of 66 to 159 °C (obsd., 8.63%; calcd., 8.57%). When the temperature holds on rising, the product lost 49.37% of the total weight in the temperature range of 157 to 341 °C, which is related to the loss of 4,4′-bipy (calcd., 49.54%). Beyond 341 °C, the 3-NPA^{2-} decomposes gradually, the products lose 32.62% of the total weight (calcd., 33.17%). The residual percentage weight at the end of the decomposition of the complex is observed as 12.04%. Then the remaining weight is assigned to MnO (obsd., 12.04%; calcd., 12.25%).

TG curve of the complex **3** is presented in Fig. 10, where one weight loss step exists and the decomposition mainly takes place in the temperature range of 67 to 602 °C. The weight loss stage may be related to the removal of 3-NPA^{2-} (found, 30.98%; calcd., 32.69%). The

residual percentage weight at the end of the decomposition of the complex is observed 68.59%, it corresponds to the PbO (calcd., 69.80%).

Conclusion

In summary, three novel coordination complexes have been synthesized by employing the rigid 3-$NPAH_2$ as the main ligand and different N-donor ligands as auxiliary ligands under hydrothermal conditions. In complexes **1–3**, the versatile 3-NPA^{2-} anions exhibit different coordination modes and coordination capacity, and connect the metal ions into different metal-carboxylates subunits with different 0D dinuclear units and 2D-layered network frameworks, which show a great effect on the formation of the final architectures. At the same time, the N-donor ancillary coligands are versatile in construction of coordination complexes. Also, the hydrogen bonds and π–π stacking also play important roles in affecting the final structure. The present different structures of complexes **1**–**2** are extended into 2D or 3D supramolecular frameworks via the hydrogen bonding and the π–π stacking interactions. In addition, the thermal decomposition process for the complexes proves that complex **3** has a good thermal stability.

Acknowledgments

The authors thank the National Natural Science Foundation of China (20761002), PR China, the Natural Science Foundation of Guangxi (053020), P.R. China, and Guangxi University for Nationalities.

Supplementary Material

Crystallographic data for the structures reported here have been deposited with CCDC (Deposition No. CCDC-941778 (**1**), No. CCDC-941779 (**2**), No. CCDC- 941780 (**3**)). These data can be obtained free of charge via http://www.ccdc.cam.ac.uk/conts/retrieving.html or from CCDC, 12 Union Road, Cambridge CB2 1EZ, UK, E-mail: deposit@ccdc.cam.ac.uk.

References

[1] (a) Perry, J. J. IV., Perman, J. A., & Zaworotko, M. J. (2009). *Chem. Soc. Rev.*, *38*, 1400. (b) Wang, Z., & Cohen, S. M. (2009). *Chem. Soc. Rev.*, *38*, 1315. (c) Dueren, T., Bae, Y. S., & Snurr, R. Q. (2009). *Chem. Soc. Rev.*, *38*, 1237. (d) Ma, L., Abney, C., & Lin, W. (2009). *Chem. Soc. Rev.*, *38*, 1248. (e) Farha, O. K., & Hupp, J. T. (2010). *Acc. Chem. Res.*, *43*, 1166. (f) Ferey, G., & Serre, C. (2009). *Chem. Soc. Rev.*, *38*, 1380.

[2] (a) Murray, L. J., Dinca, M., & Long, J. R. (2009). *Chem. Soc. Rev.*, *38*, 1294. (b) Shimizu, G. K. H., Vaidhyanathan, R., & Taylor, J. M. (2009). *Chem. Soc. Rev.*, *38*, 1430. (c) Chen, B., Xiang, S. C., & Qian, G. (2010). *Acc. Chem. Res.*, *43*, 1115. (d) Pan, M., Lin, S. M., Li, G. B., & Su, C. Y. (2011). *Coord. Chem. Rev.*, *255*, 1921. (e) Qiu, S. L., & Zhu, G. S. (2009). *Coord. Chem. Rev.*, *253*, 2891.

[3] Forster, P. M., Stock, N., & Cheetham, A. K. (2005). *Angew. Chem. Int. Ed.*, *44*, 7608.

[4] Zhou, Y. F. *et al.* (2005). *Inorg. Chim. Acta.*, *358*, 3057.

[5] Chen, S. M., Lu, C. Z., Zhang, Q. Z., Liu, J. H., & Wu, X. Y. (2005). *Eur. J. Inorg. Chem.*, *2005*, 423.

[6] (a) Lin, W., Rieter, W. J., & Taylor, K. M. L. (2009). *Angew. Chem.*, *121*, 660. (b) Jiang, H. L., & Xu. Q. (2011). *Chem. Commun.*, *47*, 3351. (c) Caskey, S. R., Wong-Foy, A. G., & Matzger, A. J. (2008). *J. Am. Chem. Soc.*, *130*, 10870. (d) Morris, R. E., & Wheatley, P. S. (2008). *Angew. Chem.*, *120*, 5044.

[7] (a) White, K. A. *et al.* (2009). *J. Am. Chem. Soc.*, *131*, 18069. (b) Law, G. L., Wong, K. L., Tam, H. L., Cheah, K. W., & Wong, W. T. (2009). *Inorg. Chem.*, *48*, 10492. (c) Lewis, D. J., Glover, P. B., Solomons, M. C., & Pikramenou, Z. (2011). *J. Am. Chem. Soc.*, *133*, 1033.
[8] Brammer, L. (2004). *Chem. Soc. Rev.*, *33*, 476.
[9] Seide, S. R., & Stang, P. J. (2002). *Acc. Chem. Res.*, *35*, 972.
[10] Caulder, D. L., & Raymond, K. N. (1999). *Acc. Chem. Res.*, *32*, 975.
[11] Lu, X. L., Wu, H., Ma, J. F., & Yang, J. (2011). *Polyhedron.*, *30*, 1579.
[12] (a) Lin, X. *et al.* (2009). *J. Am. Chem. Soc.*, *131*, 2159. (b) Zhang, X. T. *et al.* (2013). *Cryst. Growth Des.*, *13*, 792. (c) Choi, H. S., & Suh, M. P. (2009). *Angew. Chem.*, *48*, 6865.
[13] (a) Guo, F., Wang, F., Yang, H., Zhang, X. L., & Zhang, J. (2012). *Inorg. Chem.*, *51*, 9677. (b) Tsai, H. L. *et al.* (2012). *Inorg. Chem.*, *51*, 13171. (c) Lim, J. M. *et al.* (2013). *Chem. Sci.*, *4*, 388.
[14] (a) Dai, F., Dou, J., He, H., Zhao, X., & Sun, D. (2010). *Inorg. Chem.*, *49*, 4117. (b) Guo, Z. *et al.* (2009). *J. Am. Chem. Soc.*, *131*, 6894. (c) Liu, T. F., Lu, J., Guo, Z., Proserpio, D. M., & Cao, R. (2010). *Cryst. Growth Des.*, *10*, 1489.
[15] Higashi, T. (1995). *Program for Absorption Correction*, Rigaku Corporation: Tokyo.
[16] Sheldrick, G. M. (1997). *SHELXTL V5.1 Software Reference Manual, Bruker AXS, Inc.*: Madison, WI.
[17] Zang, S.-Q. *et al.* (2006). *Inorg. Chem.*, *45*, 3855.
[18] Zhang, L. *et al.* (2008). *Inorg. Chem.*, *47*, 8286.
[19] (a) Hijikata, Y. *et al.* (2011). *Chem. Commun.*, *47*, 7632. (b) Mihalcea, I. *et al.* (2011). *Inorg. Chem.*, *50*, 6243. (c) Lama, P., Sanudo, E. C., & Bharadwaj, P. K. (2012). *Dalton Trans.*, *41*, 2979.
[20] Cui, Y., Yue, Y., Qian, G., & Chen, B. (2012). *Chem. Rev.*, *112*, 1126.
[21] (a) Li, X., Sun, H. L., Wu, X. S., Qiu, X., & Du, M. (2010). *Inorg. Chem.*, *49*, 1865. (b) Hu, J. S. *et al.* (2010). *Cryst. Growth Des.*, *10*, 2676.
[22] Chen, W. *et al.* (2003). *Inorg. Chem.*, *42*, 944.
[23] Bauer, C. A. *et al.* (2007). *J. Am. Chem. Soc.*, *129*, 7136.

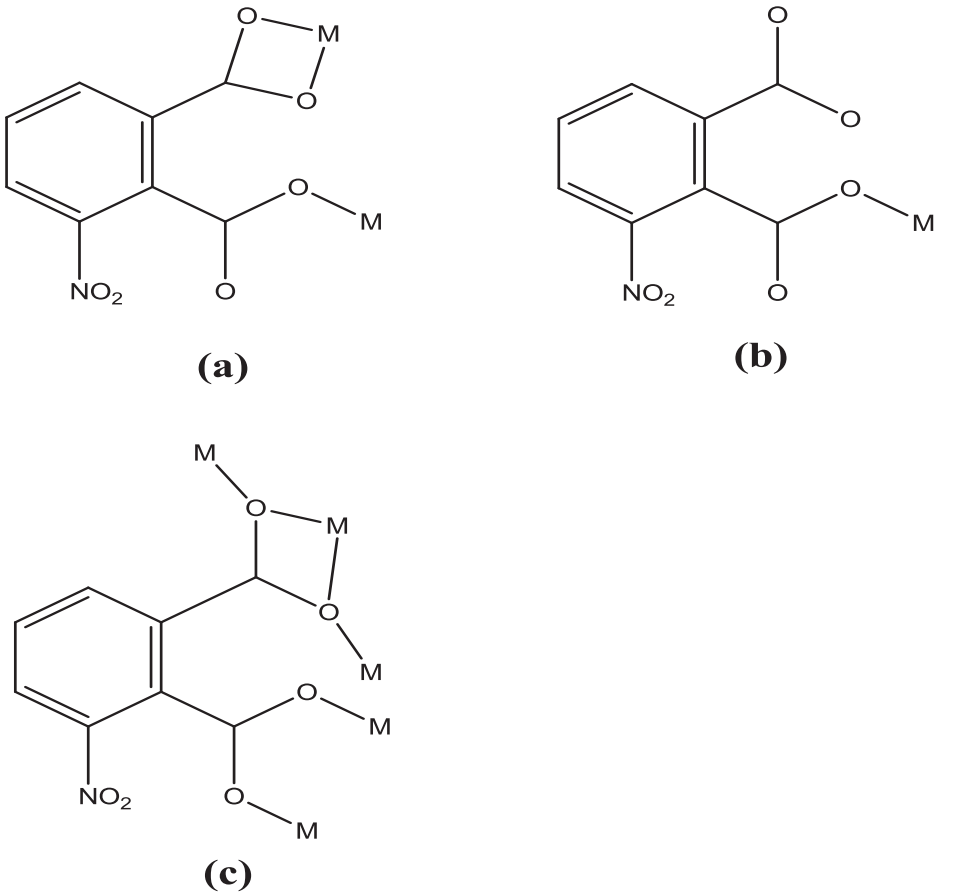

Figure S1. Coordination modes of the 3-NPA2− anion, a in 1; b in 2; c in 3.

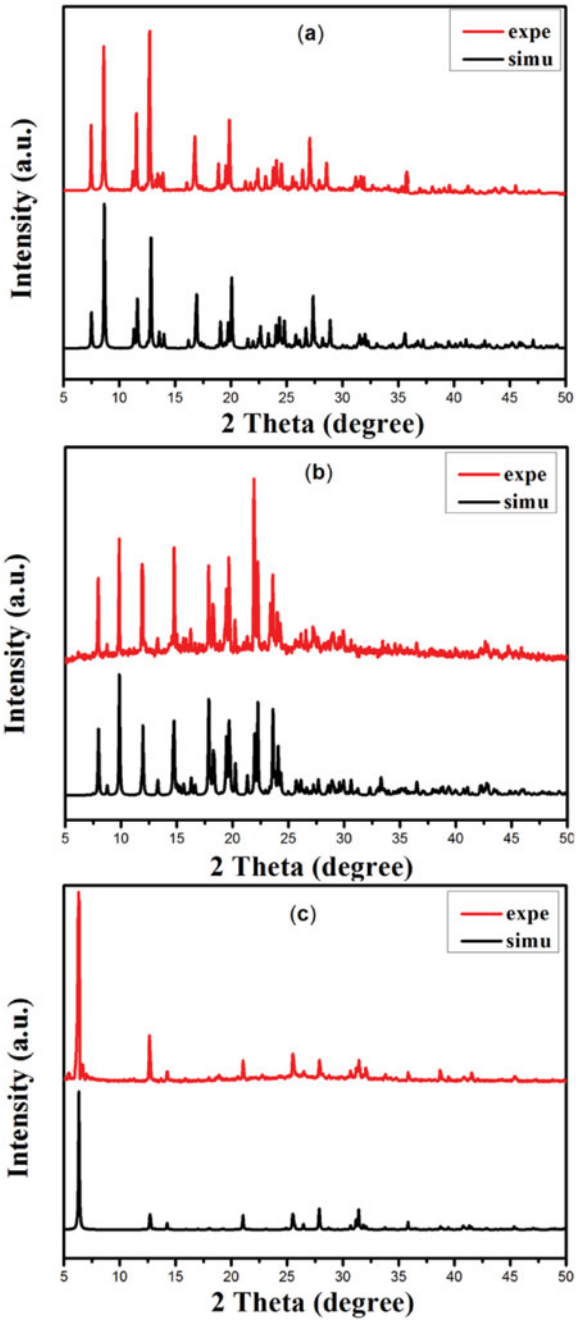

Figure S2. Simulated and experimental PXRD patterns of complex 1(a), complex 2(b), and complex 3(c).